# Variations in the spectral slope of Sgr A* during a NIR flare

S. Gillessen[1], F. Eisenhauer[1], E. Quataert[2], R. Genzel[1,3], T. Paumard[1], S. Trippe[1], T. Ott[1], R. Abuter[1], A. Eckart[4], P. O. Lagage[5], M. D. Lehnert[1], L. J. Tacconi[1], F. Martins[1]

[1] *Max-Planck-Institut für Extraterrestrische Physik, 85748 Garching, Germany*

[2] *Astronomy Department, University of California, Berkeley, CA 94720, USA*

[3] *Physics Department, University of California, Berkeley, CA 94720, USA*

[4] *1. Physikalisches Institut, Universität zu Köln, Zülpicher Str. 77, 50937 Köln, Germany*

[5] *UMR 7158, CEA-CNRS-Université Paris 7, DSM/DAPNIA/Service d'Astrophysique, CEA/Saclay, France*

## ABSTRACT

We have observed a bright flare of Sgr A* in the near infrared with the adaptive optics assisted integral field spectrometer SINFONI[1]. The observed spectrum is featureless and can be described by a power law. We show for the first time that the spectral index is correlated with the instantaneous flux and that both flux and spectral index experience significant changes within less than one hour. We argue that the near infrared flares from Sgr A* are due to synchrotron emission of transiently heated electrons, the emission being affected by orbital dynamics and synchrotron cooling, both acting on timescales of $\sim 20$ minutes. The synchrotron cooling process may account for the observed variation in spectral index, which in turn requires a magnetic field $\sim 30\,\mathrm{G}$, consistent with the equipartition field in a hot accretion flow with an accretion rate of $\sim 10^{-8}\,M_\odot/\mathrm{yr}$.

*Subject headings:* blackhole physics — Galaxy: center — infrared: stars — techniques: spectroscopic

---

## 1. Introduction

The detection of stellar orbits (Schödel et al. 2002; Eisenhauer et al. 2005; Ghez et al. 2003, 2005a) close to Sgr A* has proven that the center of our Galaxy hosts a massive black hole (MBH) with a mass of $(3.6 \pm 0.2) \times 10^6 \mathrm{M}_\odot$. Its accretion rate apparently is very low, as Sgr A* appears rather dim in all wavelengths. In the near infrared (NIR) it was detected by Genzel et al. (2003) and Ghez et al. (2004), after diffraction limited observations at the 8-m class telescopes had become possible. Usually the emission either is not visible or very weak. However, every few hours Sgr A* seems to flare in the NIR, sometimes reaching even $K \approx 15$mag. A first measurement of a flare spectrum was performed by Eisenhauer et al. (2005), showing a featureless, red spectrum (power law index in $\nu S_\nu \sim \nu^\beta$ of $\beta \approx -3$).

## 2. Observations and data reduction

We observed the Galactic Center (GC) region on 2005 June 18 from 2:40 to 7:15 UT with SINFONI (Eisenhauer et al. 2003; Bonnet et al. 2004), an adaptive optics (AO) assisted integral field spectrometer which is mounted at the Cassegrain focus of ESO-VLT Yepun (UT4). The field of view was 0.8" for individual exposures, mapped onto $64\times32$ spatial pixels. We observed in K-band, spectrally dispersed at a resolution of FWHM $5 \times 10^{-4}\,\mu$m. The first 12 integrations lasted 5 minutes each. During those we noticed NIR activity of Sgr A* and we switched to 4 minute exposures. We followed Sgr A* for another 32 exposures in this mode. In total nine integrations on a specifically chosen off-field (712" W, 406" N of Sgr A*) were interleaved. The seeing was $\sim 0.5$" and the coherence time around $3\,$ms, some short-time deteriorations excluded. The AO was locked on the closest optical guide star ($m_R = 14.65$, 10.8" E, 18.8" N of Sgr A*), yielding a spatial resolution of $\sim 80\,$mas, close to the diffraction limit of UT4 in K-band ($\sim 60\,$mas).

From all source data we subtracted the respective sky frames to correct for instrumental and atmospheric background. Next we applied flatfielding, bad pixel correction, a search for cosmic ray hits, and a correction for the optical distortions of SINFONI. The wavelength dimension was calibrated by means of line emission lamps and finetuned on the atmospheric OH-lines of the raw frames. Finally the data were assembled into cubes, taking into account atmospheric dispersion.

For all 44 cleaned cubes we extracted a collapsed image (cube median in spectral dimension) of the central part containing the three S-stars S2, S13, S17, and Sgr A*. In order to determine the flux of Sgr A* we performed a fit with five Gaussians to each of these images. Four Gaussians with a common width parameter were needed for the four sources. The fifth

Gaussian (using a width 3.5× wider) accounts for the halo of the brightest star S2. The halos of the weaker sources could be neglected. We fixed the positions of all sources (known a-priori by determining them in a combined cube) and the amplitude ratios for the stars. Five parameters were left free: An overall amplitude, the background, the width, the flux ratio halo/S2, and $\mathcal{F}$, the flux ratio Sgr A*/S2. This procedure disentangles real variability from variations in the background, the Strehl ratio, and the seeing.

As a crosscheck we determined $\mathcal{F}$ in a second way for all 44 images; for both the flare and S2 we determined the median flux in a disk (radius 4 pixels) centered on-source as well as the median flux in a 1-pixel-wide ring with inner radius 7 pixels. The difference between disk and ring flux measures the flux of the source. The such-determined values for $\mathcal{F}$ agreed very well with the values obtained from the fitting. For further analysis we used the fitted ratios. The errors are the square sum of the formal fit error and 0.03, the latter number being the typical difference between the two estimates for $\mathcal{F}$.

Our observations triggered immediate follow-up observations of VISIR, a mid-infrared (MIR) instrument mounted at ESO-VLT Melipal (UT3). From 5:25 UT on VISIR was pointing to the GC. At the position of Sgr A* no significant flux was seen. A conservative upper limit of $40\,\mathrm{mJy}$ (not dereddened) at $8.59\,\mu\mathrm{m}$ is reported (P. O. Lagage, in preparation).

## 3. Observational results

### 3.1. Light curve

The light curve of the flare (Fig. 1, left top) clearly shows intra-flare variability on timescales as short as 10 minutes. We calculated a periodogram of the light curve. While the data at hand may not be optimal for searching for periodicities (poorer sampling than our previous imaging data), it is worth noting that the highest peak in the periodogram (with a significance of $\sim 2\,\sigma$) corresponds to a period of 16 to 20 minutes. This is consistent with the timescale found by Genzel et al. (2003), who identify the quasi-periodicity with the orbital time close to the last stable orbit (LSO) of the MBH.

### 3.2. Bright state and dim state

We used $\mathcal{F}$ to define a bright ($\mathcal{F} > 0.25$) and a dim state ($\mathcal{F} < 0.25$) in the 4-minute exposures. For each of the two samples we created a combined cube in which we determined the spectral power law index $\beta$ of Sgr A*. The spectrum is obtained as median spectrum
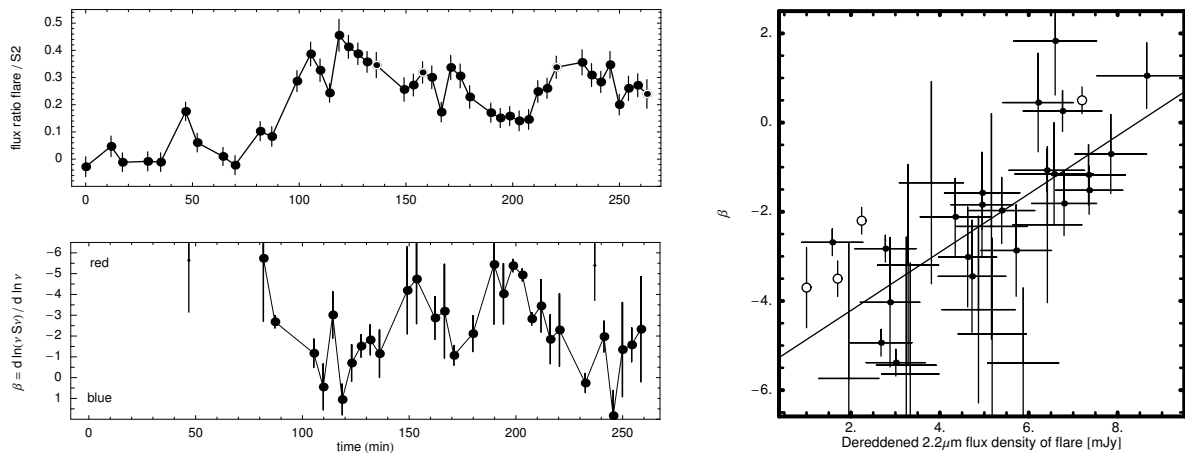
Fig. 1.— Left, top: Lightcurve of the flare, time is counted from 2:40 UT. Thin dots are exposures affected by bad seeing (FWHM$> 87 \, \text{mas}$). The peak at $t = 50 \, \text{min}$ is significant and has the largest relative flux variation. Left, bottom: Observed spectral power law index $\beta$ for the cubes which allowed for a determination. Two of the 32 points are omitted from the line to show more clearly the correlation with the flux. Right: Correlation plot of determined Sgr A* power law index $\beta$ versus flux density (filled symbols). Thick dots emphasize data points for which the error on $\beta < 1.5$. Open circles denote the data from Eisenhauer et al. (2005) - near $2 \, \text{mJy}$ - and Ghez et al. (2005b) - near $7 \, \text{mJy}$. The line is a fit to the new SINFONI data (eq. [2]).

of all pixels inside a disk with radius $r_1$ centered on source minus the median spectrum of all pixels in a 1-pixel wide ring with radius $r_2$. The result is divided by the S2-spectrum (measured in the same way) and then fit by a linear function $f$ from $2.0\,\mu$m to $2.4\,\mu$m. Finally $f$ is corrected for the temperature of S2 ($T \approx 25000\,$K). With the power law index $\beta_{\mathrm{BB}} = 3 - h\nu/(2kT) = 2.88$ of a blackbody (Rayleigh-Jeans regime) one has

$$\beta = -\frac{\ln\left(f_{2.0}/f_{2.4}\right)}{\ln(2.0/2.4)} + 2.88 \ . \tag{1}$$

With this definition, red emission has $\beta < 0$. For robustness we used a set of 21 a-priori chosen combinations where $2 \leq r_1 \leq 6$ and $5 \leq r_2 \leq 11$. The final index is obtained as the median of the 21 individual power law indices. The error is estimated by the standard deviation in the sample, rejecting outliers. We performed this procedure for Sgr A* and S17, both for the dim and the bright state cube. The result is:

| $\beta$ | S17 | Sgr A* | # of cubes |
|---:|---|---|:---:|
| bright sample | $2.7 \pm 0.9$ | $-0.9 \pm 0.4$ | 16 |
| dim sample | $3.1 \pm 1.4$ | $-3.4 \pm 1.3$ | 12 |

This shows a) that the adopted procedure gives the correct value for S17 (an early type star with a spectrum similar to S2 but a flux comparable to the flare) and b) that the flare was redder in the dim sample. It is reassuring that our values match with the results in Eisenhauer et al. (2005) who found for two weak flares ($\mathcal{F} \sim 0.15$) values of $\beta = -2.2$ and $-3.5$, and a bit redder during the rising/falling flanks. The result motivates us to look for a correlation between flux and power law index.

### 3.3. Correlation between flux and spectral index

We repeated the procedure from section 3.2 for the cubes in which the flare is detected. This yielded 32 spectral indices (Fig. 1, left bottom). The spectral index is highly correlated with the flux (Fig. 1, right). Assuming a (dereddened) flux density of 19 mJy for S2 the correlation is

$$\beta = (-5.5 \pm 0.6) + (0.65 \pm 0.11)\,S_{\mathrm{flare}}[\mathrm{mJy}] \ , \tag{2}$$

where we used $\lambda_{\mathrm{K}} = 2.2\,\mu$m and $d = 7.62\,$kpc (Eisenhauer et al. 2005). Bright flares are indeed bluer than weak flares, as suspected by Ghez et al. (2005b) and consistent with the earlier multi-band observations of Genzel et al. (2003). Our key new result is that this correlation even holds within a single event.

One might be worried about contamination effects by the S2-halo spilling light into the flare signal. If this were true, $\beta$ should be correlated with the seeing (measured by the width from the multiple fits, section 2). We did not find such a correlation. Furthermore, the measured spectral index of S17 in the individual cubes was constant. Hence, we safely exclude a contamination effect.

Interestingly, the emission at the position of Sgr A* was quite red even in the cubes before the actual flare. Inspecting older (non-flare) SINFONI data of the GC we found cases similar to the new data and other cases in which the light was identical to the local background emission. It seems necessary to discriminate between a true off-state and a quiescent state with a very red spectrum. This fits naturally into the results from section 3.3. Possibly the red quiescent state can be identified with the (variable) $3.8\,\mu$m emission detected by Ghez et al. (2004).

## 4. Interpretation

Understanding the variable emission of Sgr A* involves many processes, such as the accretion flow onto a rotating MBH (Liu et al. 2004) and synchrotron emission of relativistic electrons in it, close to the LSO (A. Eckart, in preparation). Any radiation produced propagates through strongly curved space-time as given by the Kerr metric. In order to correctly relate the emission with observations one has to consider beaming, multiple images, and Doppler shifts. Describing a complete picture is beyond the scope of this letter. However, our data clearly show that the NIR variability is caused by the combination of transient heating/acceleration with cooling and orbital dynamics of relativistic electrons.

### 4.1. Dynamical models

The timescale of $\sim 20$ minutes for the observed variations suggests orbital motion close to the LSO as one possible explanation. Recent progress has been made in simulating the effects of the Kerr metric when observing a spatially limited emission region orbiting the MBH (Paumard et al. 2005; Broderick & Loeb 2005a,b,c). Due to the Doppler effect the observed light corresponds to different rest frame frequencies depending on the orbital phase. A correlation between flux and spectral index is observed if the underlying spectrum is (concavely) curved. This is consistent with Sgr A* not having been detected at $10-20\,\mu$m (Morris et al. 2001), despite the very red NIR spectrum in the dim state. In a dynamical model the emission seen during the brightest part originates from a rest-frequency close to a

maximum of the source spectrum (where $\beta \approx 0$), the dimmer state is due to a falling flank at shorter wavelengths (where $\beta < 0$). For $v/c = 0.5$ (orbital speed at the LSO) the minimum and maximum rest-frequencies are $\nu_K/\sqrt{3}$ and $\nu_K \cdot \sqrt{3}$. Assuming a constant curvature for a range of $\Delta\beta = 0 - (-4) = 4$ yields

$$\frac{d \log_{10} \nu S_\nu}{d \log_{10} \nu} \approx -\frac{\Delta\beta}{2} - \frac{\Delta\beta}{2 \log_{10} \sqrt{3}} \log_{10} \frac{\nu}{\nu_K} \ . \tag{3}$$

Integrating and evaluating the result at the extreme frequencies yields the associated flux density variation of $\Delta S \approx 3^{\Delta\beta/2} \approx 9$. The beaming of the radiation in the direction of flight will lead to additional flux variations for the observer. For an orbiting point source the observed flux density in K-band ($\nu_K$) is given by

$$S_{\nu,\,\mathrm{obs}}(\nu_K) = S_{\nu,\,\mathrm{rest}} \left(\nu_K/D\right) D^3 \ , \tag{4}$$

where $D = \gamma^{-1}(1 - \mathbf{v} \cdot \mathbf{n}/\mathbf{c})^{-1}$ is the Doppler factor for the velocity $\mathbf{v}$ and direction $\mathbf{n}$ towards the observer. For $v/c \approx 0.5$ and an inclination of $i = 0°$ (edge-on) one has $D^3 \approx 3\sqrt{3}$. The maximum flux variation thus is $9 \cdot (3\sqrt{3})^2 = 243$. For a realistic scenario the effect is smaller: a) a value $i > 0$ reduces $D$, b) multiple images of the emission region occur, c) the exposure time is $\sim 0.25\,t_{\mathrm{orbit}}$ (average over 25% of the orbit), and d) the emission region is extended (another average). The combined effect of a) - d) is discussed in T. Paumard (in preparation). The plausible model therein reduces the relative flux variation during the flare as observed by Genzel et al. (2003) and also visible in Fig. 1 (left, top). We conclude that the effective beaming together with the concave spectrum is marginally compatible with the observed flux variations.

## 4.2. Synchrotron emission

Theoretical models predict that the mm-IR emission from Sgr A* is synchrotron emission from relativistic electrons close to the LSO. Radiatively inefficient accretion flow (RIAF) models with a thermal population of electrons ($T_e \approx 10^{11}$ K) produce the observed peak in the mm/submm but fail to produce significant flux at $2\,\mu$m (Fig. 2, left). The NIR emission requires a population of transiently heated or accelerated electrons as proposed by Markoff et al. (2001). In the following simple toy models we use a thermal electron distribution function (DF). A power law DF leads to very similar conclusions.

Figure 2 (left) shows the synchrotron emission of a model in which $\approx 1\%$ of the electrons are heated to $T_e = 2 \times 10^{12}$ K. It can account for the observed fluxes and spectral indices $\gtrsim -3$. The redder spectral indices cannot be obtained without violating the MIR upper

limits. Likewise a power law DF is consistent with the bright, blue state but not with the dim, red state. At the same time it is clear that synchrotron cooling will affect the emitting electron population. In a RIAF model (Yuan et al. 2003) the magnetic field $B$ is related to the accretion rate. For disk models with an accretion rate of $\sim 10^{-8} M_\odot$/yr (Agol 2000; Quataert & Gruzinov 2000) one has $B \approx 30$ G for $R \approx 3.5 R_S$. The synchrotron cooling time for electrons emitting at $\lambda = 2 \lambda_2 \, \mu$m in a $B = 30 B_{30}$ G magnetic field is

$$t_{\rm cool} \approx 8 \, B_{30}^{-3/2} \, \lambda_2^{1/2} \, \min \; . \tag{5}$$

This is comparable to the timescale of decaying flanks of flares as observed in Fig. 1 (right) and by Genzel et al. (2003). It is also similar to the orbital timescale, making it difficult to disentangle flux variations due to acceleration and cooling from the dynamical effects (sect. 4.1).

Once heated, the electrons rapidly cool resulting in an exponential cutoff in the NIR spectrum with a cutoff frequency decreasing with time. In Fig. 2 (middle) we show the evolution of the emitted light for the heated population during 20 minutes. This reproduces the observed range of spectral indices but predicts larger flux variations than observed. This problem can be overcome by considering mild evolution in the properties of the background plasma during the flare (Fig. 2, right). It is also plausible that there may be several components, such as a rapidly cooling spot plus an extended, less variable red component. While the examples shown are somewhat arbitrary, it is clear that an electron DF exists that can explain the very red spectral index and relatively high flux without violating the simultaneous MIR upper limit.

The estimated electron temperature ($T_e \approx 10^{12}$ K) is intriguingly similar to the virial temperature in the inner few $R_S$. This suggests that some fraction of the electrons are heated up to about the ion temperature. This could be due to non-collisional coupling between electrons and ions in localized regions of the RIAF, near shocks or in magnetic reconnection events (Begelman & Chiueh 1988). Alternatively, heating by turbulence in the RIAF may dominate over ion heating in localized regions (Quataert & Gruzinov 1999). The timescale for these processes is similar to the cooling time, explaining why the structures in the light curve are symmetric.

## 4.3. Inverse-Compton emission

The transiently heated electrons will produce inverse Compton (IC) radiation. The ratio of IC to synchrotron luminosity is the ratio of photon to magnetic energy densities. This
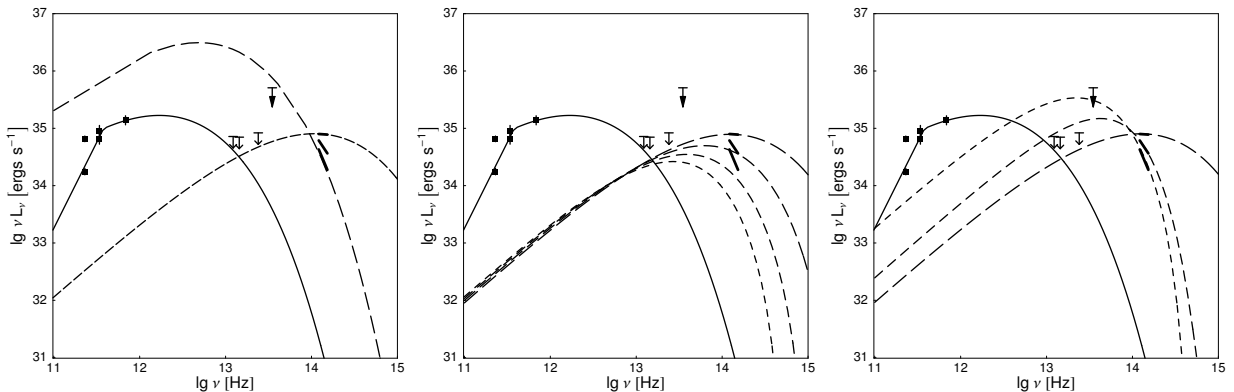
Fig. 2.— Measured fluxes of Sgr A* from the submm regime to the NIR and thermal synchrotron models. Origin of data: Range of flux densities at 230 GHz: Zhao et al. (2003); 340 GHz: D. Marrone (in preparation); 690 GHz: D. Marrone, private communication; thin plotted (non-simultaneous) upper limits $\gtrsim 10^{13}$ Hz: Morris et al. (2001); upper limit at 8.6 $\mu$m: simultaneous VISIR observations (dereddened). Our NIR data (eq. [2]) are shown as short bars for typical flux density values of 3, 5, and 8.3 mJy. The 340 GHz and 690 Hz data were measured a few days before the NIR flare. Left: Thermal synchrotron models for an emitting sphere with $R = R_S$ and $B = 30$ G. The solid line assumes $n = 2 \times 10^7$ cm$^{-3}$ and $T_e = 1.5 \times 10^{11}$ K. The short-dashed line assumes 1% of the electrons are heated up to $T_e = 2 \times 10^{12}$ K. This model can account for the bright state but a parameter set that reproduces the dim state (long-dashed curve) requires a very large electron density, yielding a MIR-flux that violates the simultaneous upper limit. Middle: The effect of synchrotron cooling for the same electron population. Average of 0-4 minutes (medium-long-), 8-12 minutes (medium-short-) and 16-20 minutes (short-dashed). While this model can explain the observed range of spectral indices it predicts larger flux variations than observed. Right: Variations of the cooling model that could explain both the NIR and the MIR data. The medium-short-dashed curve is a model which mildly increases $T$, $B$ and $n_e$ while the electrons cool for 8 minutes. The short-dashed line is a model that only increases $n_e$ (by a factor $\sim 15$) during 20 minutes.

yields for the synchrotron-self-Compton case

$$X = L_{\text{IC}}/L_{\text{sync}} \approx 7.4 \times 10^{-3} L_{35} \left( R/R_{\text{S}} \right)^{-2} B_{30}^{-2} \ , \tag{6}$$

where $L_{35}$ is the luminosity of the seed photon field in units of $10^{35}$ ergs/s. Depending on our choice of $R$ and $B$ we can - at fixed synchrotron (i.e., fixed mm/IR) luminosity - produce a wide range of IC luminosities and make the IC contribution in the NIR itself negligible.

However, IC emission can explain the two simultaneous X-ray- and IR-flares detected so far by Eckart et al. (2004) and A. Eckart (in preparation) who report similar timescales for the two wavelength regimes. This shows that the X-ray emission cannot be synchrotron light as one would expect cooling times of less than a minute (eq. 5). The X-ray emission is naturally explained by IC scattering of the transiently heated electrons. The typical $\gamma$-factor of electrons in a thermal population is given by $\gamma\, m_{\text{e}}c^2 \approx 3\,k\,T_{\text{e}}$, for the electrons emitting in the NIR $\gamma \approx 10^3$. The IC process scatters the seed photon field up according to $\nu_{\text{IC}} \approx \gamma^2\, \nu_{\text{seed}}$. Given $\gamma \approx 10^3$ and $\nu_{\text{IC}} \approx 10^{18}$ Hz for X-rays the seed photon frequency is $\nu_{\text{seed}} \approx 10^{12}$ Hz - the submm regime. The largest submm luminosity from the transiently heated electrons compatible with the MIR- and submm-data is reached for a flat synchrotron spectrum ($\beta = 0$). Thus, $L_{35} \lesssim 1$.

Via equation (6) we have $R/R_{\text{S}} \approx 8.6 \times 10^{-2}\sqrt{L_{35}/X}$. From the observed ratios $X \approx [0.1 - 1]$ we derive the upper limit $R < 0.3\,R_{\text{S}}$, meaning that in order to explain the X-ray luminosity the emission region has to be a small spot. This in turn reemphasizes the relevance of the dynamical arguments from sect. 4.1.

## REFERENCES

Agol, E. 2000, ApJ, 538, L121

Begelman, M.C. & Chiueh, T. 1988, ApJ, 332, 872

Bonnet, H. et al. 2004, ESO Messenger, 117, 17

Broderick, A. & Loeb, A. 2005, MNRAS, 363, 353

Broderick, A. & Loeb, A., preprint (astro-ph/0508386)

Broderick, A. & Loeb, A., preprint (astro-ph/0509237)

Eckart, A. et al. 2004, A&A, 427, 1

Eisenhauer, F. et al. 2003, Proc. SPIE, 4841, 1548

Eisenhauer, F. et al. 2005, ApJ, 628, 246

Genzel, R. et al. 2003, Nature, 425, 934

Ghez, A., Becklin, E., Duchene, G., Hornstein, S., Morris. M., Salim, S. & Tanner, A. 2003, ANS, 324, 527

Ghez, A. et al. 2004, ApJ, 601, L159

Ghez, A., Salim, S., Hornstein, S., Tanner, A., Lu, J., Morris, M. & Becklin, E. 2005, ApJ, 620, 744

Ghez, A. et al. 2005, ApJ, 635, in press

Liu, S., Petrosian, V. & Melia, F. 2004, ApJ, 611, L101

Markoff, S., Falcke, H., Yuan, F. & Biermann, P. L. 2001, A&A, 379, L13

Morris, M., Tanner, A., Ghez, A., Becklin, E., Cotera, A., Werner, M. & Ressler, M. 2001, BAAS, 33, 841

Paumard, T. et al., 2005, AN, 326, 568

Quataert, E. & Gruzinov, A. 1999, ApJ, 520, 248

Quataert, E. & Gruzinov, A. 2000, ApJ, 539, 809

Schödel, R. et al. 2002, Nature, 419, 694

Yuan, F., Quataert, E. & Narayan, R. 2003 ApJ, 598, 301

Zhao, J., Young, K., Herrnstein, R., Ho, P., Tsutsumi, T., Lo, K., Goss, W, Bower, G. 2003 ApJ, 586, L29